Anderson, H. R., & McGeehan, J. P. (1994). Direct calculation of coherence bandwidth in urban microcells using a ray-tracing propagation model. In 5th IEEE International Symposium on Personal, Indoor and Mobile Radio Communications (PIMRC'94), and ICCC Regional Meeting on Wireless Computer Networks (WCN). (Ch. 253 ed., Vol. 1, pp. 20 - 24). Institute of Electrical and Electronics Engineers (IEEE). doi: 10.1109/WNCMF.1994.530759, 10.1109/WNCMF.1994.530759

Direct Calculation of Coherence Bandwidth in Urban Microcells Using a Ray-Tracing Propagation Model

H. R. Anderson[1] and J.P. McGeehan
Centre for Communications Research
University of Bristol
Queen's Building, University Walk
Bristol BS8 1TR United Kingdom
Tel: 44 272 303272 FAX: 44 272 255265

Abstract - **An important parameter in characterizing radio communications channels is the coherence bandwidth. This paper presents an analysis of the coherence bandwidth in a urban microcell environment where the dynamic channel response is determined by a site-specific ray-tracing propagation model. Such an analytical model provides a direct calculation of signal fading envelope correlation as a function of frequency and location. The analysis here shows that coherence bandwidth is strongly dependent on location within a particular propagation environment and only weakly related to RMS delay spread. Typical results for frequency diversity gain for various frequency separations are also presented.**

1. Introduction

Much of the effort in designing robust and reliable communications systems focuses on choosing modulation, coding and receiver architecture schemes which mitigate the deleterious effects of the radio propagation channel. In free space, the propagation channel has a flat amplitude response (attenuation) and linear phase shift as a function frequency. When the propagation environment is not free space but contains any other elements, including the atmosphere or a single reflecting surface, the frequency response of the channel is no longer flat over all frequencies. A single reflection results in the so-called "two-ray" model in which significant nulls in the amplitude response can occur at particular frequencies depending on the reflection coefficient and ray geometry.

With highly complex propagation environments, signal energy arrives at the receiver along a variety of paths with varying amplitudes, phases, and time delays. The result is a channel frequency response which varies from place to place. One measure of the varying frequency response is the coherence bandwidth $(\Delta f)_c$. The coherence bandwidth is the frequency separation between two frequency tones which results in a given de-correlation in signal envelope amplitudes. The de-correlation is usually defined as the point where the correlation coefficient ρ_f between the fading envelopes at the two frequencies is reduce to 0.9 or 0.5. For the studies done here, a correlation coefficient of 0.9 is used to defined the correlation bandwidth. As explained in Section 2, a site-specific ray-tracing propagation model is used to find the fading envelopes and correlation coefficient.

The coherence bandwidth of the channel is particularly relevant to frequency-hopping spread spectrum (FHSS) systems[1], and to other multi-carrier systems, including OFDM. In both cases robust transmission is achieved by choosing multi-carrier frequency separations, or frequency hop distance, such that frequencies are sufficiently de-correlated that the probability of simultaneous fading impairments on multiple frequencies is low. This is the fundamental improvement which frequency diversity has to offer[2].

For the hypothetical dense urban environment studied here, coherence bandwidths ranging from 30 kHz to 130 kHz were found. The coherence bandwidth was found to be site-dependent and only weakly related to the inverse of the RMS delay spread of the power delay profile.

2. Ray-Tracing Propagation Model

A general model for the low-pass impulse response for an urban radio channel is:

$$h(t) = \sum_{n=1}^{N} A_n \delta(t - \tau_n) \exp(-j(\theta_n + \Delta\theta_n)) \quad (1)$$

in which the impulse response $h(t)$ is the sum of a set of N impulses arriving at delay times τ_n with amplitudes A_n, phases θ_n, and phase displacements $\Delta\theta_n$. The phase displacements result from the motion of the receiver or other spatial change of the receiver location relative to the rest of the propagation environment which may itself including moving objects (reflections from cars and buses, etc.). For a mobile receiver the displacement term is given by $\Delta\theta_n = (2\pi vt / \lambda)\cos(\phi_n + \phi_v)$, where φ_n is the arrival angle of the n^{th} impulse, v is the speed of motion, and ϕ_v is the direction of motion.

To use the channel model in (1), it is necessary to identify the amplitudes, time delays, and absolute phase shifts of the N components of $h(t)$. The received

[1] Also president of EDX Engineering, Inc., Eugene, Oregon USA.

components consist of the line-of-sight signal from the transmitter and a variety of signals reaching the receive antenna via reflecting surfaces, diffracting corners and scattering surfaces. By using ray-tracing techniques, the energy emitted from the source transmitting antenna is geometrically traced to determine those surfaces or corners which are illuminated. For the ray-tracing model used here, each illuminated surface is replace by an image transmitter or scattering source such that the radiation from the image represents (in amplitude, phase, and radiating directions) the energy reflected from the source. Similarly, an illuminated corner is replaced by an equivalent wedge diffraction source. With the first set of images and illuminated corners in place, each of them is then considered in turn by ray-tracing to determine the surfaces and corners they illuminate. This process is repeated for as many iterations as may be relevant to the problem at hand, or which are practical from a computational point of view. The ray interactions with the propagation environment are tracked for both HP and VP by taking into account the conductivity and permittivity of the walls and corners, and the angle of incidence for the interaction at each wall and corner.

Ray-tracing has become a widely used technique for analyzing propagation in outdoor microcells and indoor wireless LAN systems. The theoretical model used here is described in detail in [3]. Ray-tracing models along with comparisons to measurements can be found in [4] and [5].

A typical ray-tracing study for a transmitter at point AA to a receiver at point R is shown in Figure 1 along with the resulting power delay profile. As shown in [3], the magnitude and phase of the reflection and diffraction coefficients will be a strong function of the angle of incidence on the reflecting surface. The magnitude and phase of the reflection and diffraction coefficients will also depend on the frequency.

A ray-tracing propagation model only provides the ray amplitudes and phases to a single precise point. At this point it may happen that the vector sum of the rays result in a null (fade) or peak in the voltage envelope. However, in general the geometry of the environment is not known with sufficient accuracy to predict the envelope voltage so precisely. At the carrier frequencies typically involved in PCS microcell systems (around 2000 MHz), the wavelength is on the order of 15 cm. In a typical urban building database, the building wall locations may only be known within perhaps one meter. Because absolute phase can't be known, it is necessary to determine the channel response over a range of positions around the precise location where the ray-tracing analysis was performed. This can be done by considering the *fading envelope* over a range of wavelength displacements around this point. For a typical analysis, the fading voltage envelope is calculated at points spaced every 0.125 wavelengths over a range of ± 10 wavelengths in four crossing directions around the ray-tracing analysis point. This uniform pattern of four fade paths was used to reduce any anomalies which might result due to the location of the point relative to

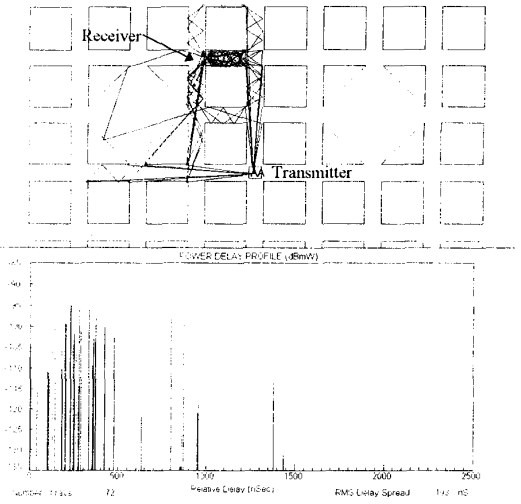

Fig. 1. Ray-tracing study with power delay profile.

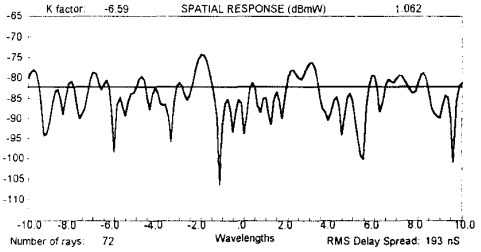

Fig. 2a. Envelope fading at 1900.000 MHz.

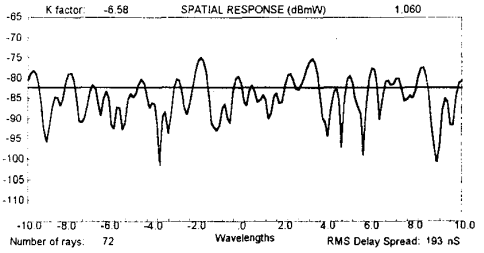

Fig. 2b. Envelope fading at 1900.100 MHz.

the physical environment and the particular ray arrival angles. With four fade paths and 160 sample points per path (every $1/8\lambda$ over $\pm 10\lambda$), a total of 640 envelope samples per ray-tracing study point were used (N=640 in equation (2)).

These fading envelopes can be created for any set of frequencies and the correlation of the envelopes at any two frequencies found by comparing the envelopes. Figure 2 shows two typical fading envelopes for frequencies separated by 100 kHz at a nominal carrier frequency of 1900 MHz. The lack of direct coincidence of many deep nulls is clear from the envelope fading examples in Figure 2.

3. Frequency Correlation Coefficient

The linear correlation coefficient between the fading envelopes at any two frequencies is given by:

$$\rho_f = \frac{\sum_n (f_1 - \bar{f}_1)(f_2 - \bar{f}_2)}{N\sqrt{\sigma_{f_1}^2 \, \sigma_{f_2}^2}} \qquad (2)$$

where $\bar{f}_1$ and $\bar{f}_2$ are the mean values of the voltage envelopes at frequencies f_1 and f_2, respectively, and $\sigma_{f_1}^2$ and $\sigma_{f_2}^2$ are the corresponding variances of the envelope waveforms, both taken across N waveform samples as described in Section 2.

Figure 3 shows an example of the correlation coefficient as a function of frequency separation for a single point on the study route in the propagation environment shown in Figure 4. For this plot and the coherence bandwidth analysis, the correlation coefficient was computer every 10 kHz of separation ranging from 0 to 400 kHz.

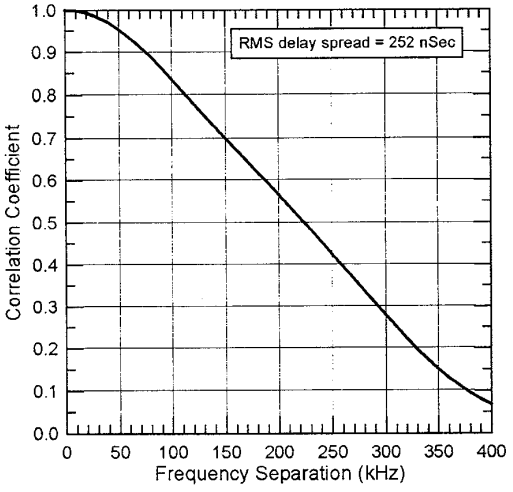

Fig. 3. Correlation coefficient vs. tone frequency separation for one point on the study route in Figure 4.

4. Coherence Bandwidth In an Urban Microcell Environment

The correlation coefficient ρ_f was calculated at a set of points along the study route shown in Figure 4. This route includes 114 points spaced at 5 meter intervals, some of which are line-of-sight with the transmitter at point AA, and some of which are shadowed are in the "plaza" area where the RMS delay spread is higher due to the widely spaced opposing reflecting surfaces. The resulting coherence bandwidth $(\Delta f)_c$ at each point along the route is plotted in Figure 5. Figure 5 shows that $(\Delta f)_c$ varies considerably as the receiver is moved along the route, with a maximum value of 130 kHz and a minimum value of 30 kHz. The average coherence bandwidth over this route is 66 kHz.

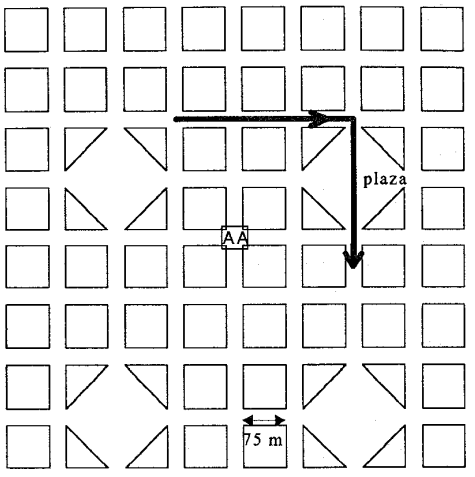

Fig. 4. Map of study route.

The relationship between coherence bandwidth and RMS delay spread is shown by the scatter plot in Figure 6. A line has been fitted through this data using the ordinary least square error (OLSE) linear curve fitting techniques. The resulting equation relating RMS delay spread and coherence bandwidth is:

$$(\Delta f)_c \cong 96 - 0.096\,\sigma_D \quad \text{kHz} \qquad (3)$$

where σ_D is the RMS delay spread in nanoseconds over the range of 100 to 500 nanoseconds.

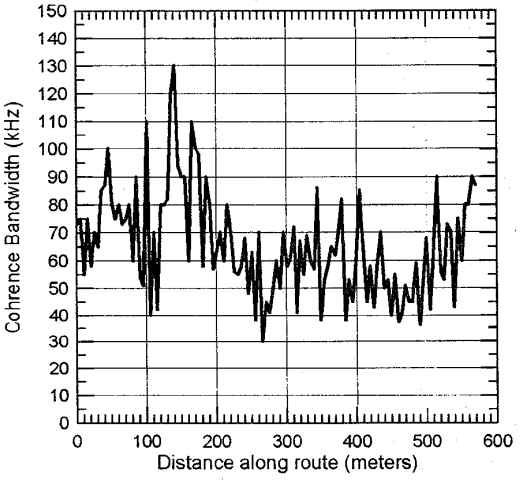

Fig. 5. Coherence bandwidth vs. distance along study route.

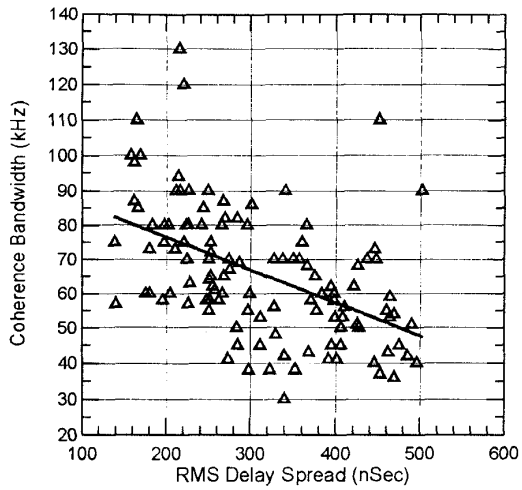

Fig. 6. Coherence bandwidth vs. RMS delay spread.

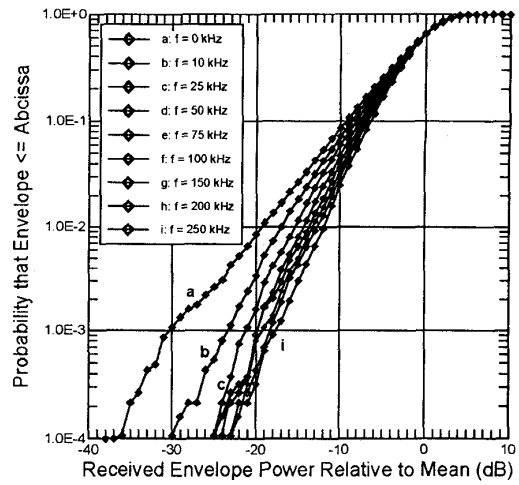

Fig. 7. CDF's of envelopes for switched frequency diversity

The RMS delay spread was found from the power delay profile in the usually way (see [3] for typical equations). The RMS delay spread also varies along the route but doesn't closely track the variations in the coherence bandwidth. This is not surprising since the RMS delay spread found from the power delay profile does not take into account the detailed phase and arrival angle information which is inherently a part of the fading envelopes used to develop the frequency correlation coefficients. Also, the RMS delay spread may be greatly affected by long-delayed low amplitude echoes. Even though such low amplitude echoes have an impact on the RMS delay spread value, they have very little impact on the actual fading voltage envelope.

This equation was derived for the specific hypothetical urban environment studied here. It may not necessarily apply to other environments. The significant point here is that RMS delay spread is only an approximate indicator of coherence bandwidth.

The treatment of coherence bandwidth in [6] showed coherence bandwidth to be a much stronger function of RMS delay spread. However, the analysis in [6] assumed a hypothetical exponential delay profile rather than the more realistic profiles derived from the ray-tracing propagation model. The ray-tracing model as applied to the particular environment here does exhibit a weakness in that due to its limited overall dimensions, RMS delay spreads greater than 500 nSec are rarely produced. Higher RMS delay spreads are common in the environments treated in [6].

5. Frequency Diversity Gain

Because of the lack of correlation between the fading envelopes at different frequencies, two separated frequencies can be combined to achieve diversity gain. Common diversity combining technique include switched (selection), equal gain, or maximal ratio. For the research done here, simple switched diversity was used. In simple switched diversity the amplitude of the signals on the diversity branches are continuously compared and a the branch with the higher amplitude signal selected.

Diversity improvement is usually assessed in terms of diversity gain; i.e., the equivalent transmitter power increase in dB that would be needed to achieve the same system performance improvement as the diversity scheme provides. The diversity gain can usually be determined from the cumulative distribution function (CDF's) of the envelopes before and after diversity combining. As an example, the CDF's of the fading envelopes distributions for all the envelopes for all the points on the study route in Figure 4 are plotted in Figure 7. In this figure the left-most line is the CDF distribution of the fading envelope for a frequency separation of 0 kHz. The other lines show the CDF's of the resulting envelope when the two frequencies are separated by amounts ranging from 10 to 250 kHz. This figure clearly shows that diversity gain increases with increasing frequency separation. For a 250 kHz frequency separation in this particular propagation environment, the diversity gain achieved is essentially the same as that achieved with two independent Rayleigh-fading diversity branches[7]. The fading envelope CDF's in Figure 7 can be further used to estimate the diversity improvement in bit error rate following the approach found in [8].

6. Conclusions

A method for finding the coherence bandwidth in an dense microcell environment using a ray-tracing propagation model has been presented. Using this model it is possible to develop realistic fading envelope patterns for different frequencies. By comparing the envelopes, the degree of correlation between them and hence, the coherence bandwidth can be estimated.

The results show that in the hypothetical urban environment studied here, the coherence bandwidth ranged from 30 kHz to 130 kHz. The average coherence bandwidth is 66 kHz. The coherence bandwidth was found to be loosely related to the inverse of the RMS delay spread.

The signal envelopes developed at separated frequencies with the ray-tracing propagation model were also analyzed as a two-branch switched diversity system. The results show that diversity gain increases with increasing frequency separation, as expected. For a frequency separation of 250 kHz in the hypothetical urban microcell environment used here, the frequency diversity gain is nearly the same as two independent Rayleigh fading diversity branches.

7. Acknowledgment

The authors would like to thank Andy Nix of the Centre for Communication Research at the University of Bristol for many discussions which were helpful in carrying out this research.

8. References

[1] D. J. Purle, A.R. Nix, M.A. Beach, and J.P. McGeehan, "A preliminary performance evaluation of a linear frequency hopped modem," *Proceedings of the 1992 Veh. Tech. Society Conf.*, Denver, pp. 120-124, May 1992.

[2] J. Proakis. *Digital Communications*. New York: McGraw-Hill, 1989, p. 265.

[3] H.R. Anderson, "A ray-tracing propagation model for digital broadcast systems in urban areas," *IEEE Trans. on Broadcasting*, Vol. 39, no. 3, Sept. 1993, pp. 309-317.

[4] K.S. Schaubach, N.J. Davis and T.S. Rappaport, "A ray-tracing method for predicting path loss and delay spread in microcell environments," *Proceedings of the 1992 Veh. Tech. Society Conf.*, Denver, pp. 932-935, May 1992.

[5] M.C. Lawton and J.P. McGeehan, "The application of GTD and ray launching techniques to channel modelling for cordless radio systems," *Proceedings of the IEEE Veh. Tech. Conf.*, Denver, pp. 125-130, May 1992.

[6] W.C. Jakes. *Microwave Mobile Communications*. IEEE Press: Piscataway, New Jersey. 1994. (re-published). pp. 45-60.

[7] M. Schwartz, W.R. Bennett, and S. Stein. *Communication Systems and Techniques*. New York: McGraw-Hill, 1966, pp. 434-440.

[8] H.R. Anderson, A.R. Nix, and J.P. McGeehan. "Theoretical Polarization Diversity Studies In An Urban Microcell Environment," *Proceedings of the Fourth International Symposium on Personal, Indoor, and Mobile Radio Communications*, Yokohama, Japan, Sept. 1993.